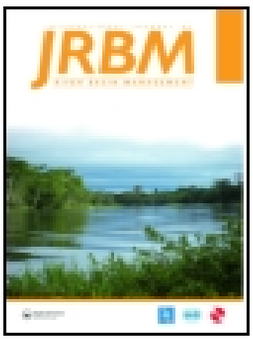

International Journal of River Basin Management

ISSN: 1571-5124 (Print) 1814-2060 (Online) Journal homepage: http://www.tandfonline.com/loi/trbm20

Numerical simulations of turbulent flow around side-by-side circular piles with different spacing ratios

Ali-Asghar Beheshti, Behzad Ataie-Ashtiani & Hamed Dashtpeyma

To cite this article: Ali-Asghar Beheshti, Behzad Ataie-Ashtiani & Hamed Dashtpeyma (2017): Numerical simulations of turbulent flow around side-by-side circular piles with different spacing ratios, International Journal of River Basin Management, DOI: 10.1080/15715124.2017.1280811

To link to this article: http://dx.doi.org/10.1080/15715124.2017.1280811

Published online: 07 Feb 2017.

INTL. J. RIVER BASIN MANAGEMENT, 2017
http://dx.doi.org/10.1080/15715124.2017.1280811

Taylor & Francis
Taylor & Francis Group

Numerical simulations of turbulent flow around side-by-side circular piles with different spacing ratios

Ali-Asghar Beheshti[a], Behzad Ataie-Ashtiani[b] and Hamed Dashtpeyma[b]

[a]Department of Water Resources Engineering, Ferdowsi University of Mashhad, Mashhad, Iran; [b]Department of Civil Engineering, Sharif University of Technology, Tehran, Iran

ABSTRACT

Numerical simulations of the turbulent flow around single and side-by-side piles at different spacing ratios (centre-to-centre distance to the pile diameter) with flow Reynolds number of 10^5 on the fixed flat-bed are presented. The calculations are performed using the computational fluid dynamics model, FLOW-3D, which solves the Navier–Stokes equations in three dimensions with a finite-volume method. The numerical results of time-averaged flow patterns around single and side-by-side piles are validated using the available experimental measurements. At the downstream of the single pile, dimensionless vortex shedding frequency (Strouhal number) is estimated as 0.22. The maximum values of bed shear stress around side-by-side piles at different spacing ratios are compared with the maximum values obtained for the single pile. Interactions of horseshoe vortices on different cases of side-by-side piles are studied. Numerical results show that the critical arrangement for which the largest bed shear stress was observed is the case with the spacing ratio of 3.

ARTICLE HISTORY
Received 13 June 2016
Accepted 28 December 2016

KEYWORDS
Turbulent flow; flow patterns; computational fluid dynamics; side-by-side piles

Introduction

Turbulent flow field and scour development due to the flow around man-made and natural pile structures are among important concerns in many engineering and environmental problems. Two important examples are scour-hole development around bridge piers (Ataie-Ashtiani and Beheshti 2006, Ataie-Ashtiani *et al.* 2010) and river flow interaction with vegetation (Vandenbruwaene *et al.* 2011, Bouma *et al.* 2013). Stability of bridges can be affected by the instability of their foundations on the river current. One of the most important factors of infrastructure pier instability is scouring around their foundation in facing of flow current (Ahmed and Rajaratnam 1998). A great number of researches have been performed on finding the empirical equations to predict the maximum scour-hole depth around bridge foundations (e.g. Melville and Coleman 2000, Sheppard *et al.* 2004, Arneson *et al.* 2012). Melville and Coleman (2000) presented design formula for local scour depth (y_s) estimation around single piles based on K-factors.

$$y_s = K_h K_I K_d K_s K_\alpha K_t, \tag{1}$$

where K_h is the flow depth-pile size factor, K_I is the flow intensity factor, K_d is the sediment size factor, K_s is the pile shape factor, K_α is the pile alignment factor, and K_t is the time factor. Sheppard *et al.* (2004) expressed a state-of-the-art equation for predicting scour depth at a single pile. The equation for clear-water condition is given as follows:

$$\frac{y_s}{D} = 2.5 f_1\left(\frac{h}{D}\right) f_2\left(\frac{U}{U_c}\right) f_3\left(\frac{D}{d_{50}}\right), \tag{2}$$

where y_s is the maximum scour depth, h is the flow depth, D is the pile diameter, U is the flow mean velocity, U_c is the critical flow velocity, and d_{50} is the grains mean diameter. The functions of $f_1(h/D)$, $f_2(U/U_c)$, $f_3(D/d_{50})$ are presented by Sheppard *et al.* (2004). The proposed equation in America Highway Administration (FHWA, Circular HEC-18) to estimate the maximum scour depth can be expressed as (Arneson *et al.* 2012) follows:

$$\frac{y_s}{h} = 2.2\, K_1 K_2 K_3 \left(\frac{D}{h}\right)^{0.65} Fr^{0.43}, \tag{3}$$

where Fr = Froude number and K_1, K_2, and K_3 are the correction factors for pier nose shape, angle of attack of the flow, and bed condition, respectively. However, the predictions with these equations show an overestimation of the scour depth related to the experimental data for different conditions (Melville 1975, Dargahi 1990, Ataie-Ashtiani and Beheshti 2006). This inadequacy of the predicted scour depth using these equations could be related to the lack of understanding about the flow patterns and turbulence in these events. Most of the damages on the bridges occur under the flood conditions when the flow is fully turbulent and different from experimental conditions. Therefore, investigations with high Reynolds numbers can be more realistic and useful (Khosronejad *et al.* 2012). Scouring can be described by extra shear stress exertion on the bed. The exertion of shear stress, on the other hand, is wide ranging in different flow regimes. For instance, in turbulent flow, the turbulent viscosity depends on turbulent intensity. Consequently, the study of the flow patterns and shear stress distributions around piles is necessary for acquiring better intuitions about the scour initiation and development (Ahmed and Rajaratnam 1998, Akbari and Price 2005, Dey and Raikar 2007, Lam *et al.* 2008, Baranya *et al.* 2012, Baykal *et al.* 2015).

As a matter of the fact that the flows around the piles in a group have a great interaction with each other, the results of flow field around single piles cannot be generalized to group piles (Sumner *et al.* 1999). Recently, there is an increasing research attention to the scour-hole development around pile groups (e.g., Coleman 2005, Ataie-Ashtiani and Beheshti

CONTACT Ali-Asghar Beheshti beheshti@um.ac.ir

2006, Ataie-Ashtiani *et al.* 2010, Beheshti *et al.* 2013, Lança *et al.* 2013, Beheshti and Ataie-Ashtiani 2016a, 2016b) and the influences of piles geometry on the flow field and scouring conditions (Hannah 1978, Salim and Jones 1998, Liu *et al.* 2001, Akbari and Price 2005, Carmo and Meneghini 2006, Palau-Salvador *et al.* 2008, Papaioannou *et al.* 2008, Gopalan and Jaiman 2015). While pile groups and complex piers are commonly employed in engineering projects (e.g. bridge foundations), the interaction of flow patterns and its effect on the scouring around such geometries has not comprehended appropriately. One of the experimental studies in this field was performed by Ataie-Ashtiani and Beheshti (2006) and Beheshti and Ataie-Ashtiani (2010) based on the experimental analysis of flow field and scouring around complex and group piles. They found that the maximum scour depth around two side-by-side piles with the spacing ratio of $G/D = 3$ is 20% larger than that of the single pile. Here, G is the center-to-center distance between the piles of diameter D. An exhaustive review on the experimental investigation of two circular cylinders in cross-flow is performed by Sumner (2010), who categorized previous studies into three configurations, namely tandem, side-by-side, and staggered according to the different arrangements of cylinders. One of the most important findings of this study is that the investigation of flow characteristics with different Reynolds numbers is still needed.

By the fact that the experimental analysis based on the time-averaged results cannot show the real gradient of velocities, many researchers tend to investigate this problem with numerical approaches. One of the first applicable investigations in this field was performed by Richardson and Panchang (1998) using the computational fluid dynamics model FLOW-3D. They used the k-epsilon as a turbulent model in computing the eddy viscosity. They considered the flow pattern around single circular pile on flat, intermediate, and final equilibrium scoured bed. The bed was modelled as a rigid surface with a conical shape for scour-hole. This assumption for scour-hole shape made scepticism on correctness of the actual flow patterns around the pile (Richardson and Panchang 1998). Ali and Karim (2002) performed numerical analysis for flow around a single circular pile using FLUENT. For simplicity, they modelled the free surface as a smooth wall. This assumption cast doubt on the accuracy of the final result by the fact that the free surface profile for this flow is not flat (Ali and Karim 2002). One of the important studies on numerical analysis of flow pattern around single piles is conducted by Salaheldin *et al.* (2004). They compared different turbulent models such as standard k-epsilon, RNG k-epsilon, realizable k-epsilon, and Reynolds stress model (RSM). They compared their results with some benchmark flow measurements in the laboratory. The results showed that the realizable k-epsilon was unable to provide accurate results in comparison with the standard and RNG k-epsilon or RSM models (Salaheldin *et al.* 2004). However, it should be noted that the realizable k-epsilon has generally been shown to produce equal or better results than standard k-eps in many other studies; hence, this result may be special for the single-pile case. Ge and Sotiropoulos (2005) conducted numerical modelling of flow around a complex pier using a finite-volume method to solve unsteady Reynolds-averaged Navier–Stokes (URANS) equations. The Reynolds number based on the width of the upstream pier was $Re = 2.37\times10^7$. Their method was capable of resolving the unsteady vortex shedding and identifying the location of the large-scale vortices (Ge and Sotiropoulos 2005). Kirkil *et al.* (2008) performed large-eddy simulations and conducted experiments on the flow structure around a circular cylinder on a scoured bed. Based on their findings, the consistency between the numerical and experimental results was acceptable. They found that the separation of the shear layer near the bed was delayed with respect to the far region from the bed (Kirkil *et al.* 2008).

Table 1 summarizes some numerical studies of flow around single piles and pile groups. On the review of the previous numerical studies, it can be realized that most of the numerical simulations have some limitations; some of them conducted with simplifications, most of them paid attention to single cylindrical piles, and some studies performed with a low flow Reynolds number. As it is obvious on the basis of nonlinear behaviour of the flow in different domains and different regimes, further investigations for turbulent flow around pile groups are still required (Beheshti and Ataie-Ashtiani 2016b).

This study is a numerical analysis of turbulent flow around side-by-side pile groups on the rigid bed. Numerical analysis is performed by FLOW-3D that solves the Navier–Stokes equations using a finite-volume method with collocated grids (Flow Science 2012). The main objective of the present study is to assess the structure of the turbulent flow in order to find the critical ratios of pile spacing related to the highest exertion of the instantaneous shear stress on the bed. Other objectives of the paper are to discuss the turbulent conditions around the piles and to examine the numerical modelFLOW-3D in simulation of the flow filed around single and side-by-side piles with a high Reynolds number.

Problem description

Geometry and domain of our numerical simulations are based on Ataie-Ashtiani and Aslani-Kordkandi's (2012, 2013) experimental work. Their experiments were performed for single and double piles in a channel with 15 m length, 1.26 m width, and 0.9 m depth at the Hydraulics Laboratory in Civil Engineering Department at the Sharif University of Technology, Tehran, Iran. Piles were placed in the sediment recess and the recess was filled with uniform sand of median size, d_{50}, 0.71 mm. The nylon-made piles had a diameter, D, of 9.1 cm, and the centre-to-centre distance of two piles, G, was equal to 27.3 cm ($G/D = 3$). They measured the $3D$ instantaneous velocities by an acoustic Doppler velocimeter. The numerical domain for side-by-side piles with $G/D = 2$ is shown in Figure 1; the computational domain extends $11D$ upstream of the pile and $22D$ downstream of it. The domain width and height are $13.8D$ and $4.4D$, respectively. In the Cartesian coordinates, the origin was located on the bed at the intersection of the channel line of symmetry (x direction) and the line passing the centres of the piles (y direction). The piles modelled as solid objects and placed through the mesh with a diameter of 9.1 cm. The upstream extension of computational domain from pile centre ($11D$) considered in order to provide a fully developed flow (Bauer 1954). The bed modelled as a thin layer with a surface roughness of 0.17 cm. The roughness height was considered approximately as 2.5 d_{50}, as suggested by Bennett (1995). The mean sediment size of $d_{50} = 0.71$ mm was selected based on the experimental conditions. The flow depth (h) is

Table 1. Selected numerical studies of flow around bridge piles.

Researchers	*Re*	Method	Section	Bed condition
Gopalan and Jaiman (2015)	1.66×10^5	URANS–LES	Tandem cylinders	Rigid
Baykal *et al.* (2015)	$(3.3–5.1) \times 10^4$	3D URANS	Circular cylinder	Rigid, movable
Akbari and Price (2005)	800	2D, Navier–Stokes equation	Circular – staggered cylinder pairs	Rigid
Bao *et al.* (2012)	100	Second-order characteristic-based split finite elements	Square-group piles	Rigid
Baranya *et al.* (2012)	53,500	3D RANS, nested grids	Circular-group piles	Rigid
Bosch and Rodi (1998)	22,000	Finite-volume and two layer approaches	Square-single	Rigid
Carmo and Meneghini (2006)	160–320	3D and 2D, spectral element method	Circular-tandem	Rigid
Khosronejad *et al.* (2012)	63,000–29,000	3D, URANS	Square, circular, rhomboid-single	Movable
Kirkil *et al.* (2008)	18,000	LES	Circular-single	Movable
Lam *et al.* (2008)	100–200	3D, finite volume	Circular-four cylinders	Rigid
Liu *et al.* (2001)	200	ARMA, finite element	Circular-elastic Cylinders-side-by-side	Rigid
Palau-Salvador *et al.* (2008)	42,000–1400	3D, LES	Circular-tandem	Rigid
Papaioannou *et al.* (2008)	160	2D, DNS	Circular-tandem	Rigid
Roulund *et al.* (2005)	$100 - 2 \times 10^6$	3D, EllipSys3D	Circular-single	Movable

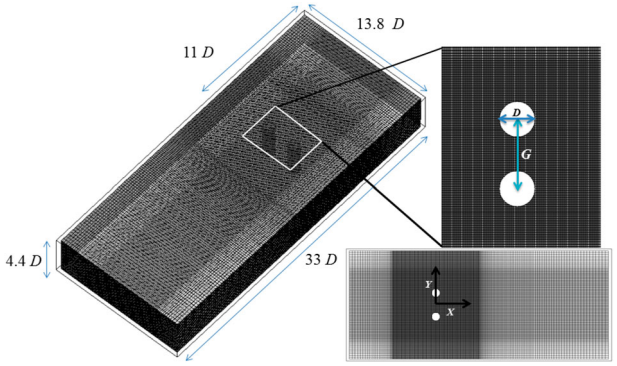

Figure 1. Geometry, mesh, and dimensions of numerical domain for side-by-side piles.

3.6*D* with the average flow rate (*Q*) of 134 L/s and corresponding approach flow velocity (U_0) of 33 cm/s (see Table 2).

The Reynolds number of the flow in numerical analysis and available experimental data is 10^5 ($Re = U_0\ h/\nu$), and the Froude number ($Fr = U_0/\sqrt{gh}$) is about 0.18, that shows a turbulent and subcritical flow conditions (Ataie-Ashtiani and Aslani-Kordkandi 2012, 2013). As a matter of fact that the piles surface in experiments is not completely smooth, for more accurate results in the numerical analysis, the surface roughness of the piles is determined as 0.01 times of the bed roughness. The same computational domain is used for both side-by-side piles and single pile with the same diameter. Numerical simulations were conducted for three different spacing ratios of *G*/*D*= 3.5, 3, and 2.5 on the same domain as illustrated in Figure 1.

Numerical modelling approach

Mathematical formulations

FLOW-3D solves the equations such as heat transfer or motion by finite-volume and finite-difference approaches (Smith and Foster 2005). The code uses rectangular grids that let users refine the mesh by defining a plane in the regions of interest for more detailed results. The structured and rectangular meshes are advantageous in that they can be generated easily and fast. Moreover, these grids have higher stability in numerical models (FLOW-3D User Manual, Flow Science 2012). The important equations of motion that this code is based on are continuity equation, momentum equations, fluid interfaces, and free-surfaces (Hirt and Nicholas 1981, Flow Science 2012). The differential equations are written in the terms of Cartesian coordinates (*X*, *Y*, *Z*). The general mass continuity equation is (Flow Science 2012)

$$V_f \frac{\partial \rho}{\partial t} + \frac{\partial}{\partial X}(\rho U A_X) + R\frac{\partial}{\partial Y}(\rho V A_Y) + R\frac{\partial}{\partial Z}(\rho W A_Z) + \xi \rho u A_X = R_{DIF} + R_{SOR}, \quad (4)$$

where V_f is the fractional volume, ρ is the fluid density, R_{DIF} is the turbulent diffusion term, and R_{SOR} is the mass source, (*U*, *V*, *W*) are velocity components in (*X*, *Y*, *Z*) coordinates, respectively, *A* is a fractional area open to flow, and ξ is a term for definition of coordinate system (equal to 0 for Cartesian system and 1 for Cylindrical system). The turbulent diffusion term on the right side (first term) is defined as (Flow Science 2012)

$$R_{DIF} = \frac{\partial}{\partial X}\left(\nu_\rho A_X \frac{\partial \rho}{\partial X}\right) + R\frac{\partial}{\partial Y}\left(\nu_\rho A_Y R \frac{\partial \rho}{\partial Y}\right) + \frac{\partial}{\partial Z}\left(\nu_\rho A_Z \frac{\partial \rho}{\partial Z}\right) + \xi \frac{\rho \nu_\rho A_X}{X}, \quad (5)$$

where $\nu_\rho = c_p\ \mu/\rho$, μ is viscosity and c_p is a constant whose reciprocal is usually referred to as the turbulent Schmidt number. The Navier–Stokes equations used in FLOW-3D are (Flow Science 2012)

$$\frac{\partial U}{\partial t} + \frac{1}{V_f}\left(U A_X \frac{\partial U}{\partial X} + V A_Y R \frac{\partial U}{\partial Y} + W A_Z \frac{\partial U}{\partial Z}\right) - \xi \frac{A_Y V^2}{X V_f} = -\frac{1}{\rho}\frac{\partial p}{\partial X} + G_X + f_X - \frac{R_{SOR}}{\rho V_f}(U - U_w - \delta U_s), \quad (6)$$

$$\frac{\partial V}{\partial t} + \frac{1}{V_f}\left(U A_X \frac{\partial V}{\partial X} + V A_Y R \frac{\partial V}{\partial Y} + W A_Z \frac{\partial V}{\partial Z}\right) - \xi \frac{A_Y U V}{X V_f} = -\frac{R}{\rho}\frac{\partial p}{\partial Y} + G_Y + f_Y - \frac{R_{SOR}}{\rho V_f}(V - V_w - \delta v_s), \quad (7)$$

$$\frac{\partial W}{\partial t} + \frac{1}{V_f}\left(U A_X \frac{\partial W}{\partial X} + V A_Y R \frac{\partial W}{\partial Y} + W A_Z \frac{\partial W}{\partial Z}\right) = -\frac{1}{\rho}\frac{\partial p}{\partial X} + G_Z + f_Z - \frac{R_{SOR}}{\rho V_f}(W - W_w - \delta W_s), \quad (8)$$

Table 2. Model properties of present study.

Domain length	Domain width	Domain height	h	U_0	D	Reynolds number	Froude number
3 m (33D)	1.26 m (13.8D)	0.4 m (4.4D)	0.325 m (3.6D)	0.33 m/s	0.091 m (D)	10^5	0.18

where (G_x, G_y, G_z) are body accelerations, (f_x, f_y, f_z) are viscous accelerations, and the final terms on the right sides of these equations indicate the injection of mass at a source represented by geometry components. Fluid configurations are defined in terms of a volume of fluid (VOF) function, $F(x, y, z, t)$ (Hirt and Nicholas 1981). In the fluid interfaces and free surface, the equation representing the VOF per unit volume is (Flow Science 2012)

$$\frac{\partial F}{\partial t}+\frac{1}{V_{\mathrm{f}}}\left(\frac{\partial}{\partial X}(FA_X U)+R\frac{\partial}{\partial Y}(FA_Y V)\right.$$

$$\left.+\frac{\partial}{\partial Z}(FA_Z W)+\xi\frac{FA_X U}{X}\right)=F_{\mathrm{DIF}}+F_{\mathrm{SOR}}, \quad (9)$$

$$F_{\mathrm{DIF}}=\frac{1}{V_{\mathrm{f}}}\left\{\frac{\partial}{\partial X}\left(\nu_{\mathrm{f}}A_X\frac{\partial F}{\partial X}\right)+R\frac{\partial}{\partial Y}\left(\nu_{\mathrm{f}}A_Y R\frac{\partial F}{\partial Y}\right)\right.$$

$$\left.+\frac{\partial}{\partial Z}\left(\nu_{\mathrm{f}}A_Z\frac{\partial F}{\partial Z}\right)+\xi\frac{\nu_{\mathrm{f}}A_X F}{X}\right\}, \quad (10)$$

where $\nu_{\mathrm{f}}=c_{\mathrm{f}}\,\mu/\rho$, c_{f} is a constant whose reciprocal is sometimes referred to as a turbulent Schmitt number, and F_{SOR} is a mass source(Flow Science 2012).

The turbulent model used in this study is the k-epsilon RNG model. The turbulence kinetic energy (K) and its rate of dissipation (ϵ) are formulated as follows (Smith and Foster 2005, Flow Science 2012):

$$\frac{\partial K}{\partial t}+u_j\frac{\partial K}{\partial x_j}=\tau_{ij}\frac{\partial u_j}{\partial x_j}-\epsilon+\frac{\partial}{\partial x_j}\left[\frac{1}{\rho}\left(\mu+\frac{\mu_t}{\sigma_K}\right)\frac{\partial K}{\partial x_j}\right], \quad (11)$$

$$\frac{\partial \in}{\partial t}+u_j\frac{\partial \in}{\partial x_j}=C_{\in 1}\frac{\in}{K}\tau_{ij}\frac{\partial u_i}{\partial x_j}-C_{\in 2}\frac{\in^2}{K}$$

$$+\frac{\partial}{\partial x_j}\left[\frac{1}{\rho}\left(\mu+\frac{\mu_t}{\sigma_\epsilon}\right)\frac{\partial \epsilon}{\partial x_j}\right], \quad (12)$$

where t is the time, u_i, u_j are mean velocities along X and Y directions, respectively,τ_{ij} is Reynolds-stress tensor, ε is the dissipation rate, μ_t is the eddy viscosity, x_i,x_j are lengths in X and Y directions, σ_K is a constant equal to 1, and $C_{\in 1}$, and $C_{\in 2}$ are constants. Eddy viscosity is defined as (Smith and Foster 2005, Flow Science 2012)

$$\mu_{\mathrm{t}}=\frac{\rho C_\mu K^2}{\in}, \quad (13)$$

where C_μ is a constant equals to 0.09 (Smith and Foster 2005, Flow Science 2012).

Boundary conditions

In this study, the inflow (the section with minimum value of X) is defined as specified velocity with stagnation pressure related to the flow elevation. Stagnation pressure is defined on the inlet. As mentioned before, the piles are located at a distance far enough from the inlet so that the flow approaching the piles was fully developed flow. At the outflow (the section with the maximum value of X), a stagnation pressure related to the flow elevation and zero fluid fraction is defined in order to block the backflow. Planes with the minimum and maximum values of Y are defined as side walls. The bed is modelled as a thin fixed layer with a specified roughness height ($k_{\mathrm{s}}=2.5d_{50}$). The plane with the maximum value of Z is defined as specified zero pressure to represent the free surface. At the piles, a wall function is used. FLOW-3D uses the combination of the logarithmic law of the wall for rough and smooth walls (Smith and Foster 2005). Parallel component of velocity adjacent to the wall (u_0) is computed as follows (Smith and Foster 2005, Flow Science 2012):

$$u_0=u_*\left[\frac{1}{k}\ln\left(\frac{\rho u_* d}{\mu}\right)+5.0\right], \quad (14)$$

where u_* is the local shear velocity, k is the von Karman constant, and d is estimated to be half of the cell width in the wall normal direction.

Mesh independency analysis

In this section, numerical analysis for single pile is presented with various sizes of grid cells ranging from a coarse grid (case 1 in Table 3) to a refined grid (case 4 in Table 3). The comparison of results obtained from cases 3 and 4 show negligible differences. As an example, Figure 2 shows the velocity profiles of U obtained from different cases in a point located in the downstream region for checking the mesh independency. As can be seen from Figure 2, differences between the results obtained from cases 3 and 4 are negligible in a point located at the downstream of the pile. In this study, the mesh generation of case 3 is used for further simulations, in order to have less computational time. Figure 3 compares the results obtained using different cases of mesh generations with experimental results at two points located upstream and downstream of the side-by-side piles with $G/D=3$. As can be seen from Figure 3, case 3 gives reasonable agreement between experimental and numerical results for both single and side-by-side piles. For both side-by-side and single-pile

Table 3. Specification of different mesh sizes for mesh independency analysis.

	Case 1	Case 2	Case 3	Case 4
Size of cells around pile in the x direction	0.54D	0.1D	0.073D	0.066D
Total number of cells in the x direction	60	200	250	300
Size of cells around pile in the y direction	0.22D	0.1D	0.073D	0.066D
Total number of cells in the y direction	52	104	160	180
Size of cells around pile in the z direction	0.22D	0.1D	0.073D	0.066D
Total number of cells in the z direction	20	40	60	100
Size of nearest cell to bed (z direction)	0.22D	0.1D	0.073D	0.066D
Total number of cells	6.2×10^4	8.3×10^5	2.4×10^6	5.4×10^6

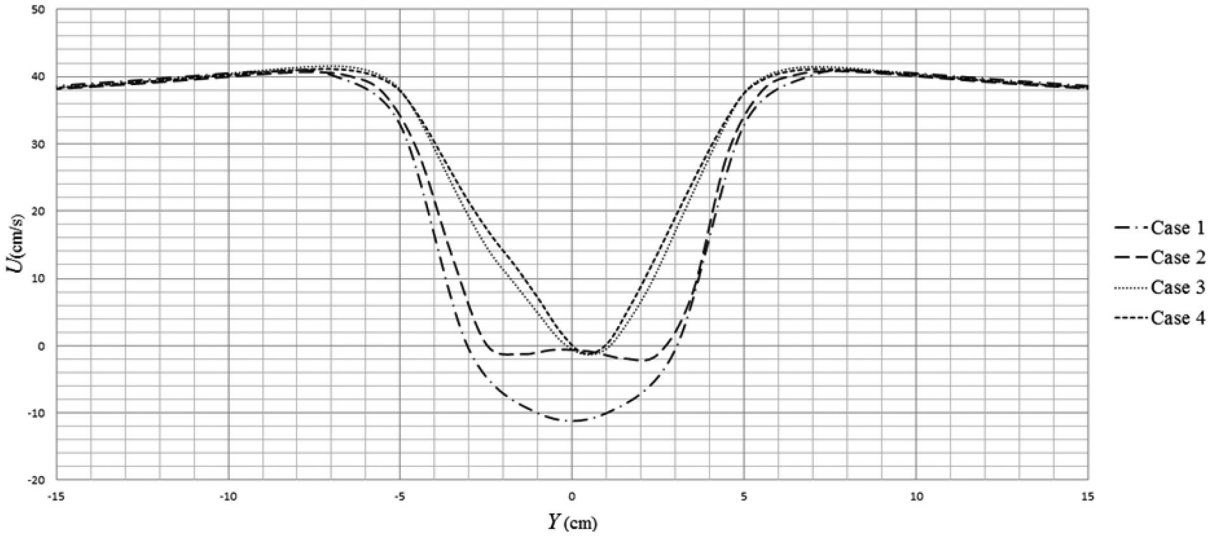

Figure 2. Profiles of U in the Y direction at $X = 0.6D$ and $Z = 2D$ for different cases of mesh size for single pile.

models, the mesh is refined in a region of $5.5D$ in the X direction and $4.4D$ in the Y direction from the centre (Figure 1).

Validation of numerical simulation

The velocity contours and velocity profiles obtained from numerical simulations of flow around single pile and side-by-side piles with $G/D = 3$are compared with the experimental results of Ataie-Ashtiani and Aslani-Kordkandi (2012, 2013). The experimental results are presented in time averaged form (Ataie-Ashtiani and Aslani-Kordkandi 2012, 2013). For the sake of comparison, the time-averaged numerical results are considered. Numerical simulations are performed under the same conditions of the experiments with the same geometry and flow conditions. In order to validate the numerical model, the velocity profiles at different points located in upstream and downstream regions close to the piles as well as the velocity contours in the plane $Z = 2D$ are compared with experimental

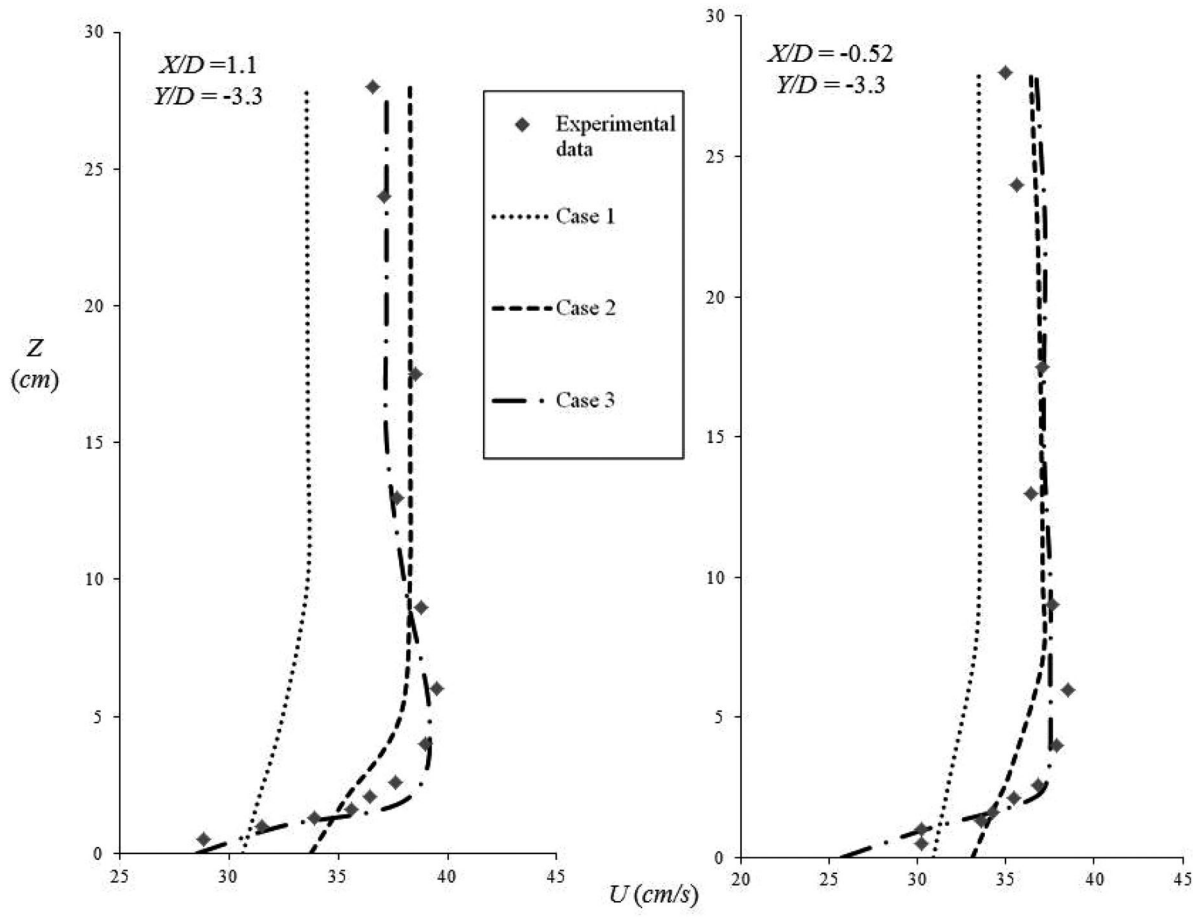

Figure 3. Comparison of time-averaged velocity profile of U obtained using different cases of mesh generations and experimental measurements at two points located upstream and downstream of the side-by-side piles with $G/D = 3$.

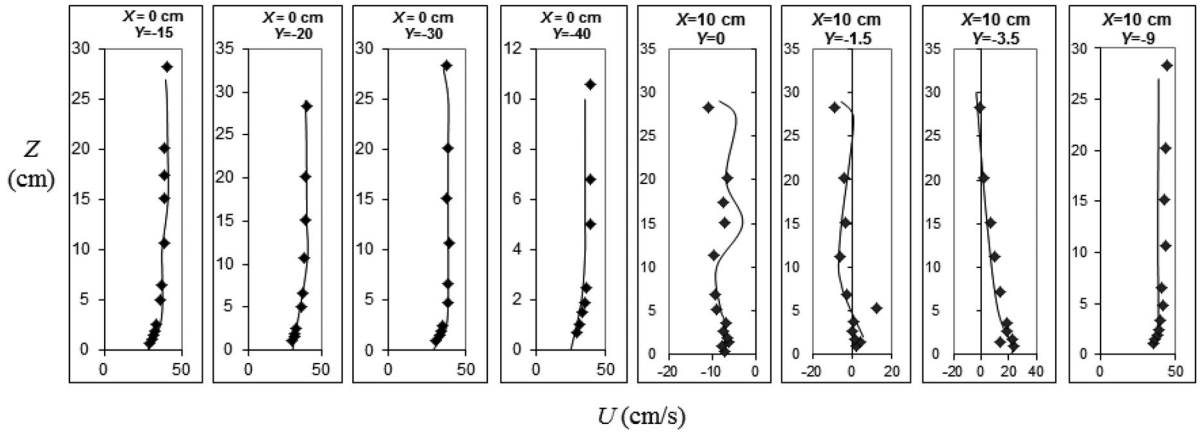

Figure 4. Profiles of averaged *U* along the *Z* coordinate at the upstream and downstream of the single pile, experimental results (dots), and numerical results (line).

measurements. Results show acceptable correlation between the numerical simulations and experiments in both cases of single and side-by-side piles. Velocity profiles obtained from numerical simulations and experimental measurements around the single pile are shown in Figure 4. It can be seen that the main features of the flow around the single pile are simulated accurately. Moreover, Figure 5 compares the time-averaged velocity profiles of U from both numerical and experimental results at different points around side-by-side piles with G/D = 3. As seen from Figures 3–5, fairly good agreement with experiments regarding the main flow features was obtained in both upstream and downstream regions using case 3 simulations. In addition, the streamwise (U) and transverse (V) velocity contours obtained on the plane $Z = 2D$ for side-by-side configuration with $G/D = 3$ are compared with experimental measurements in Figure 6. Owing to the symmetry in the domain and averaging processes, the flow patterns around both piles must be the same.

Velocity gradients of the numerical results near to the bed have a satisfactory similarity to the experimental ones. As illustrated in Figure 6, the velocities around both piles obtained from numerical and experimental investigations show similar patterns; hence, the adequacy of numerical analysis for side-by-side piles can be confirmed.

Results and discussions

Single pile

Numerical simulation of flow patterns around single pile is performed as the benchmark for numerical validation and comparing the flow features of the side-by-side cases with that of the single pile. Owing to the high Reynolds number, the oscillations and vortex shedding were expected. The dimensionless vortex shedding frequency (S_t=fD/U_0, f is vortex shedding frequency) in the wake zone downstream of the pile is found to be 0.22, on the basis of time history of X-velocity (U) at the point with coordinates (8.5, 8.5, 20) cm through 50 s from beginning of the simulation. The first 10 s of simulation is not considered, considering the fact that the influence of initial conditions in the domain is not cleared, and the flow patterns are not shaped thoroughly in this period of time (Figure 7).

The vortices in the front side and lateral sides can exert extra shear stress on the bed. The primary vortices in the mean flow around a single pile are visualized using the Q-criterion (Dubief and Delcayre 2000). Figure 8 shows the iso-surfaces of Q shaded with the Z-vorticity (right) and the contours of shear stress on the bed (left). As it is illustrated, it can be concluded that the maximum exertion of shear stress takes place in the front half in the lateral part

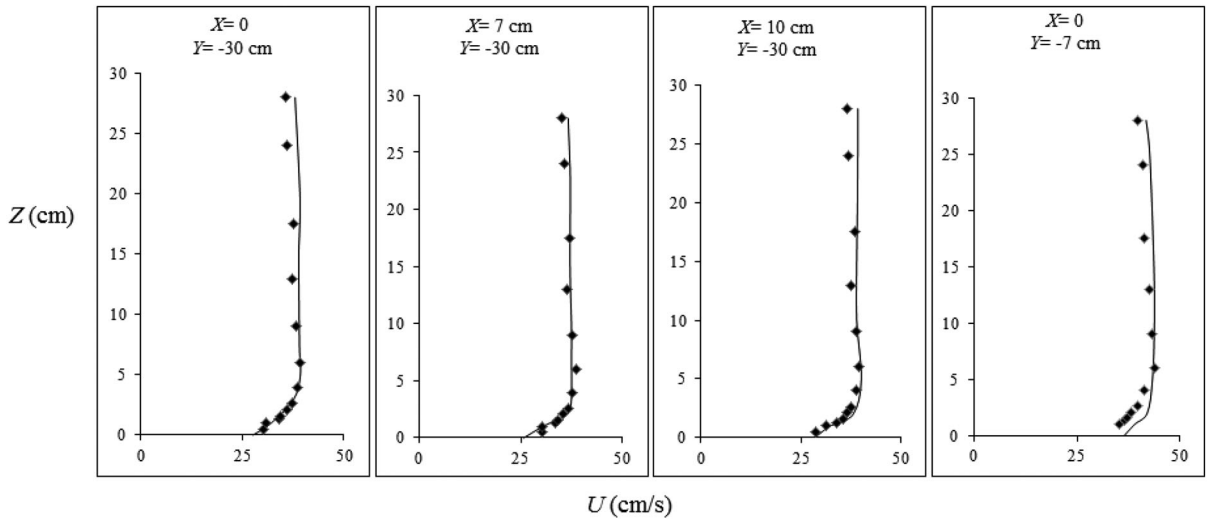

Figure 5. Profiles of averaged *U* along the *Z* coordinate at the upstream and downstream of the side-by-side piles in the case $G/D = 3$ obtained from experimental results (dots), and numerical results (line).

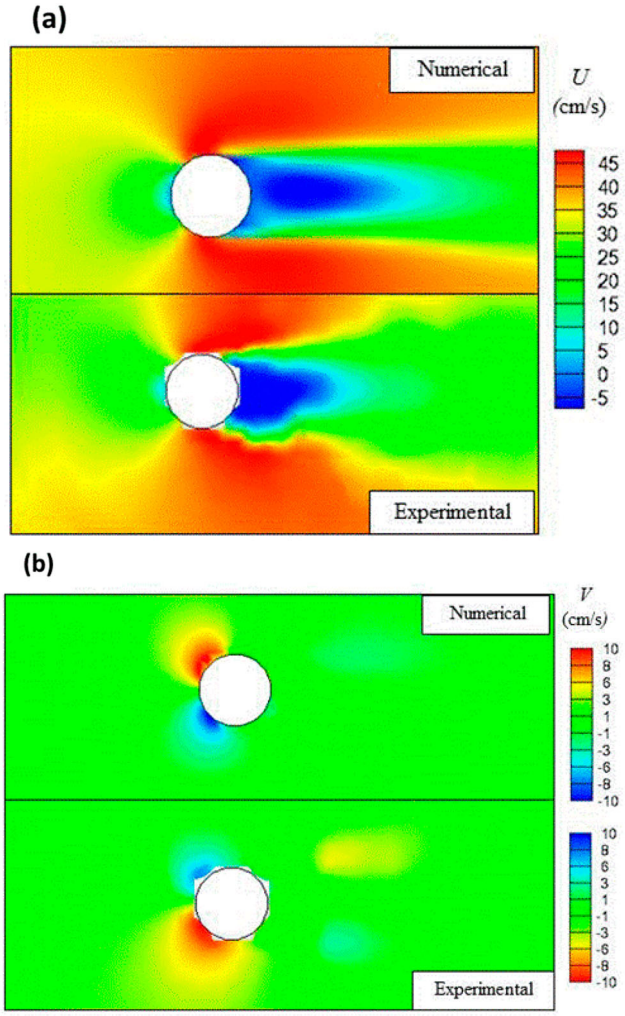

Figure 6. Experimental (bottom) and numerical (top) results of (a) streamwise and (b) transverse velocity contours on the plane $Z = 2D$ around side-by-side piles with $G/D = 3$.

of the pile due to the creation of horseshoe vortices. In comparison with the piles in laminar flows, the separation point of the boundary layer is delayed. This is consistent with the findings of other researchers for the case of turbulent flow around circular piles (Roulund *et al.* 2005, Kirkil *et al.* 2008) (Figure 8). This delay of separation can be attributed to high exchange of momentum between the layers of fluid in the separating turbulent boundary layer (Roulund *et al.* 2005) (Figure 8).

Side-by-side piles

The flow pattern around pile groups is different from that of the single piles as a result of complex interactions between flow structures around them (Ataie-Ashtiani, and Beheshti 2006, Ataie-Ashtiani and Aslani-Kordkandi 2012, 2013, Bao *et al.* 2013). Hence, due to a nonlinear behaviour of the flow, the results that are obtained from a single pile case cannot be extended into a group of piles. A variety of pile group arrangements can bring about variety in flow behaviours and patterns. The main patterns are the flow interference leading to enhanced flow speeds or turbulence between side-by-side piles and sheltering of piles in tandem arrangements (Akilli *et al.* 2004, Ataie-Ashtiani and Aslani-Kordkandi 2012, 2013, Bao *et al.* 2012). One of the most important factors to consider is the ratio of G/D. In this study, three G/D for side-by-side piles including 2.5, 3, and 3.5 are examined. At the end, the critical ratio on the basis of higher shear stress exertion is defined. All the contours and graphs are presented at the critical moment (the moment when the maximum exertion of shear stress occurs).

Figure 9 shows the iso-surface of Q shaded with the Z-vorticity. As it is illustrated, the inner legs of the horseshoe vortices have highest interaction to each other for the case with $G/D = 2.5$. The interaction between the legs of the horseshoe vortices decreases as G/D increases. The vorticity can show the general rotating behaviour of the flow. One of the most important characteristics of turbulent flow is the vortex stretching that caused by the vorticity. More stretched vorticity illustrates higher gradient and higher potential to energy cascade. Energy cascade transports energy from large eddies to small ones. Iso-surface of vorticity in the X or Y direction and vortex stretching can show the strength of the turbulence and the structure of the flow. Small eddies have a higher

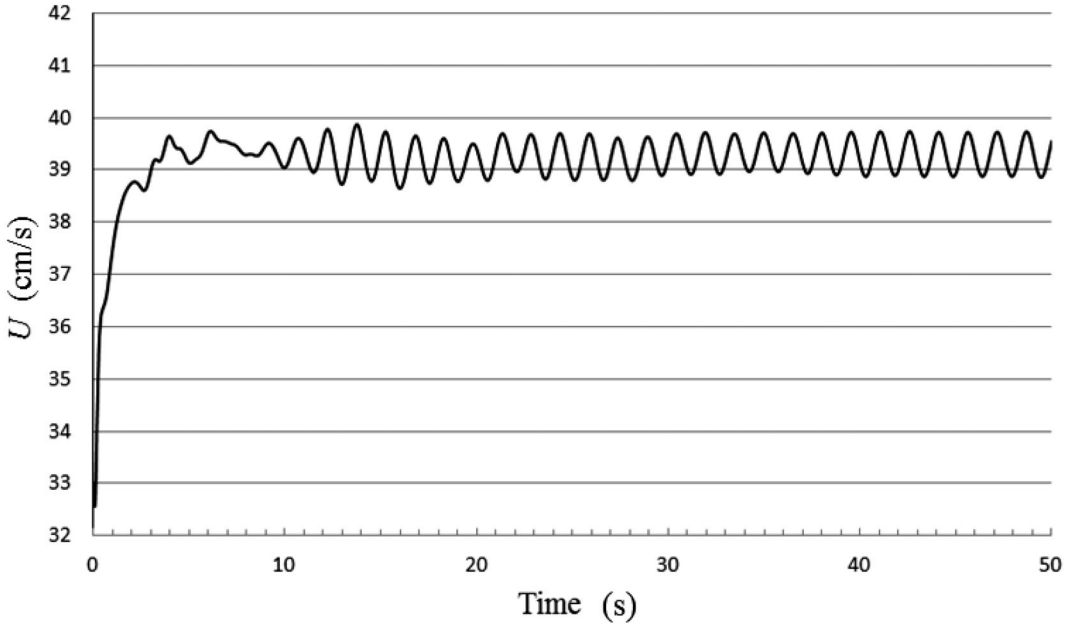

Figure 7. Time history of U at point ($0.9D$, $0.8D$, $2D$) for single pile.

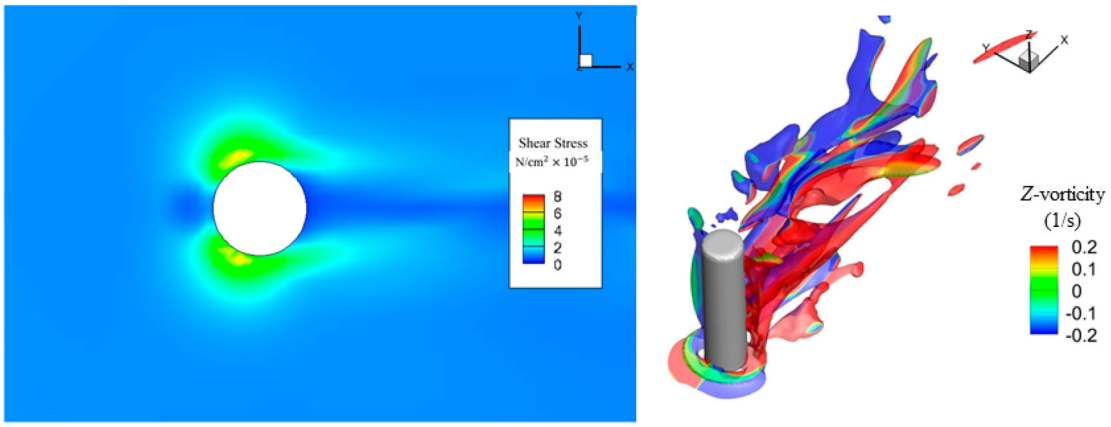

Figure 8. Contours of shear stress on the bed (left) and iso-surfaces of *Q* shaded with the *Z*-vorticity contours (right) for single pile at critical moment.

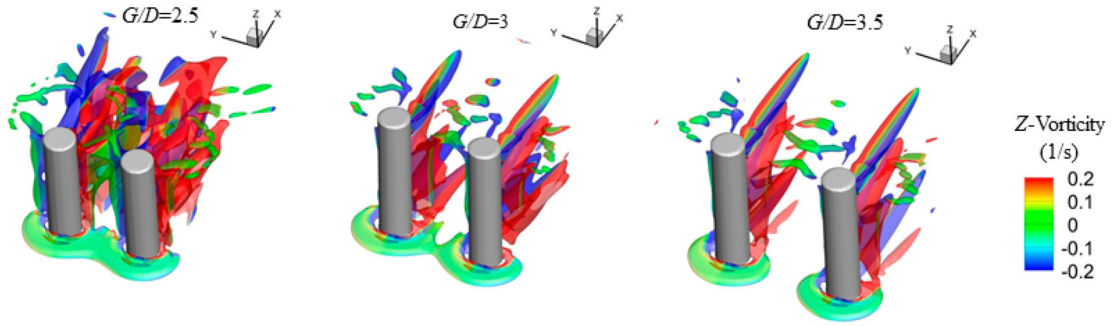

Figure 9. Iso-surfaces of *Q* shaded with the *Z*-vorticity contours for side-by-side piles with different spacing ratios at critical moment.

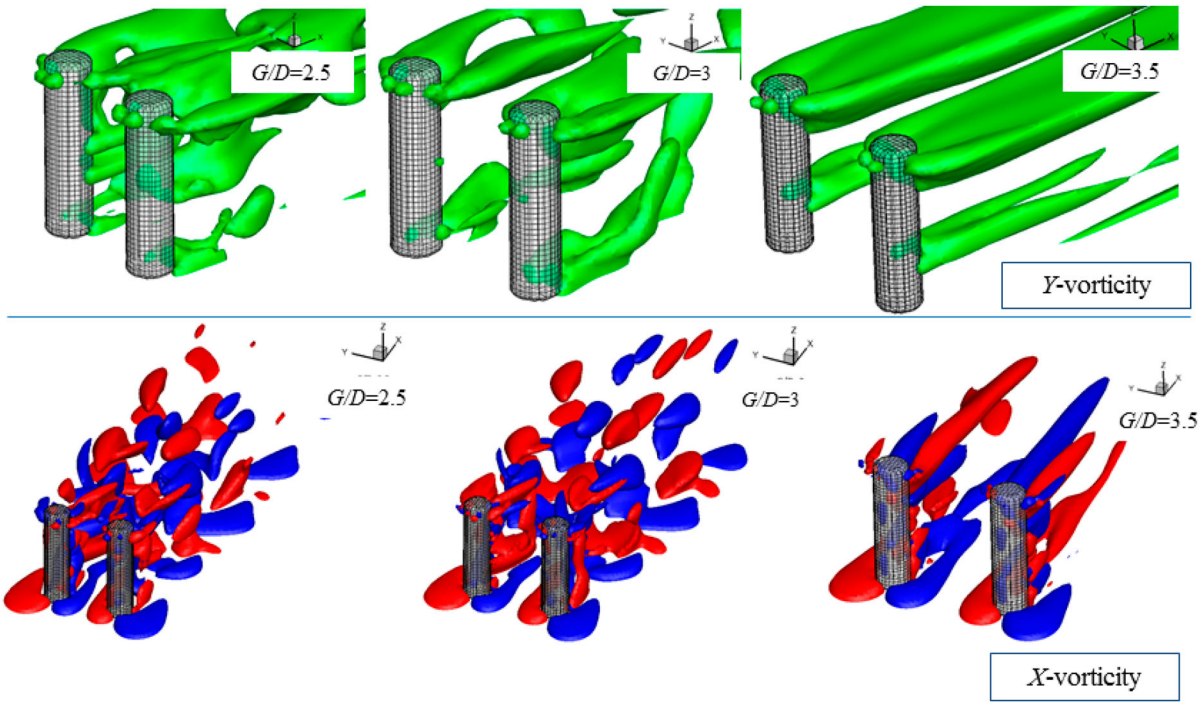

Figure 10. Iso-surfaces of *Y*-vorticity at critical moment (U_p), and iso-surfaces of *X*-vorticity at a value of −0.9 1/s (sullen) and 0.9 1/s (pastel) at critical moment (Bottom) for side-by-side piles with different spacing ratios.

frequency and result in a higher gradient as they attached to the bed. Therefore, an extra shear stress exertion on the bed can be expected. As it can be concluded from Figure 10, the case with $G/D = 3.5$ has a patch of the high value of *Y*-vorticity at a higher elevation with respect to the other cases, then on the basis of this phenomenon, lower shear stress exertion on the bed can be expected for this case. In the case with $G/D = 3$, larger areas of the high value of *Y*-vorticity is stuck to the bed. It can be seen that the lower *G/D* causes larger oscillations. As it can be seen from iso-surfaces of the vorticity, the vortices are stretched due to the turbulent flow and then dissipated when they become small enough (Figure 10). The

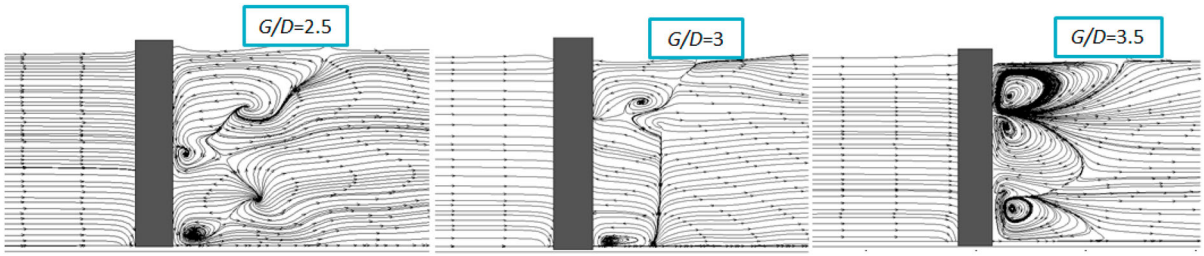

Figure 11. Streamlines of flow around side-by-side piles at the vertical section crossing the centres of left piles at critical moment.

vorticity at the upstream of the piles shows the existence of vortices at this region. Similarly, in the case of a single pile, these vortices are reported by other researchers such as Kirkil *et al.* (2008), Dargahi (1989), and Ataie-Ashtiani and Aslani-Kordkandi (2012, 2013).

When flow approaches the piles, it separates into three parts. The part which passes through the middle of the piles is contracted and it is called the contraction flow. Smaller G/D does not mean a more powerful contraction flow or more critical condition for shear stress exertion in any cases, as the interaction of separated layers from both piles makes resistance for passing the flow through the piles. Shear stress exertion on the bed is critical in a specific G/D due to the fact that in the very large or small (near to zero) ratios the shear stress exertion can be reduced. This is due to the fact that when the space between the piles becomes too large or too small, oscillations cannot occur more intensively as a result of a lower interaction of eddies or smaller amplitude of vortices oscillations.

Figure 11 shows that when shedding starts from one pile, at the critical moment, there are some differences on locations and numbers of vortices that are shaped at vertical planes crossing the centres of the piles. At the case $G/D = 3$, one of the vortices is shaped very close to the bed which can exert higher shear stresses on it. At $G/D = 2.5$, that vortex shaped at a higher elevation with a weaker strength.

Table 4. Maximum and minimum of parameters in whole domain for different spacing ratios.

	$G/D = \infty$	$G/D = 2.5$	$G/D = 3$	$G/D = 3.5$
u_{max}	1.46 U_0	1.55 U_0	1.53 U_0	1.57 U_0
u_{min}	−0.58 U_0	−0.66 U_0	−0.60 U_0	−0.57 U_0
v_{max}	0.81 U_0	0.93 U_0	0.84 U_0	0.88 U_0
v_{min}	−0.81 U_0	−0.93 U_0	−0.84 U_0	−0.88 U_0
w_{max}	0.38 U_0	0.57 U_0	0.51 U_0	0.65 U_0
w_{min}	−0.38 U_0	−0.56 U_0	−0.52 U_0	−0.44 U_0
S_t	0.22	0.21	0.21	0.2
τ_{max}	τ_s	1.13 τ_s	1.40 τ_s	1.16 τ_s

The contours of shear stress on the rigid bed for cases of $G/D = 2.5$, 3, 3.5 are compared to each other. Due to the fact that the shear stresses measured by using the averaged velocity is not completely precise (Huang *et al.* 2009), in the present study the instantaneous velocities with actual gradients are considered. However, there are some acceptable researches that are performed based on the time-averaged results with some considerations (Snyder and Castro 1999, Nikora and Goring 2000, Song and Chiew 2001, Ge *et al.* 2005).

Figure 12 shows that the shear stress exertion on the bed in the case of $G/D = 3$ is more critical than other cases. Exerted shear stress on bed for the case $G/D = 3$ is about 1.4, 1.24, and 1.21 times larger than that of the single pile, the case with $G/D = 2.5$, and the case with $G/D = 3.5$, respectively. Consequently, it can be recognized that the ratio of $G/D = 3$ is the critical ratio for the cases studied here. Figure 13 illustrates that the amplitude of oscillation at the downstream region decreases as G/D increases (Bao *et al.* 2013). By increasing G/D, the oscillations at the downstream of each pile happen symmetrically with a lower amplitude (Akilli *et al.* 2004, Bao *et al.* 2013). For a lower G/D, the oscillations occur more intensively. For the case of $G/D = 3$, on the other hand, the oscillation of V is more powerful with higher amplitude in comparison to the other cases (Figure 13).

Table 4 shows the maximum and minimum values of the velocities in different directions in the whole domain. In addition, the maximum values of bed shear stresses are presented in this table as a factor of maximum bed shear stress for a single pile case. It is stated that the maximum shear stress exertion on the bed occurs at the case with $G/D = 3$. Interestingly, the maximum velocities are not observed for the case with $G/D = 3$. Rather, the maximum velocities occurred between the piles for the case $G/D = 2$. More uniform velocity profiles and the higher shear stress exertion on the case with $G/D = 3$ show the higher intensity of the mixing effect and the higher momentum exchange between the layers of the fluid. The highest shear stress exertion in this

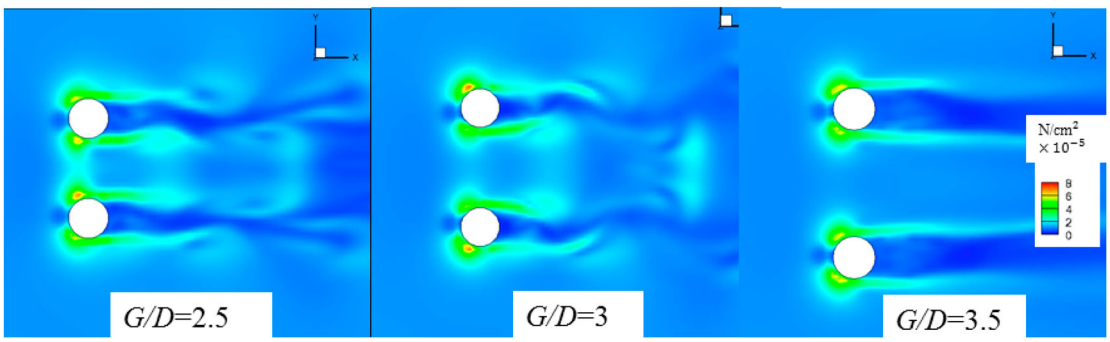

Figure 12. Contours of shear stress on the bed for side-by-side piles with different G/D at critical moment.

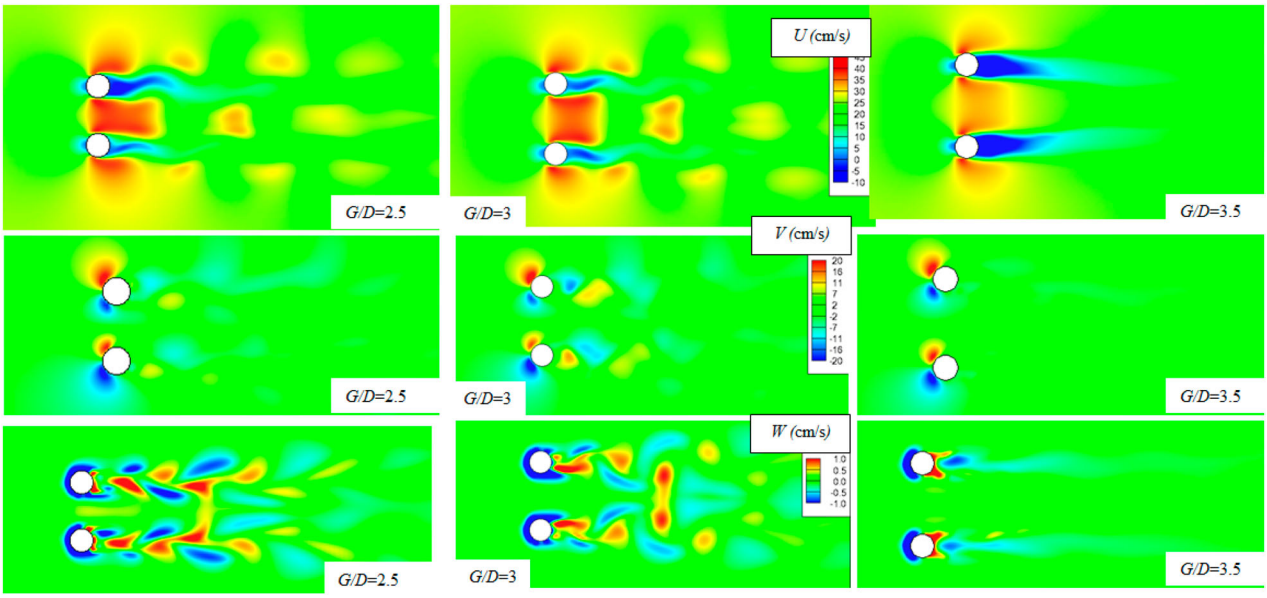

Figure 13. Contours of U (up), V (middle), and W (bottom) on the plane $Z = 0.1D$ around side-by-side piles with $G/D = 2.5$ (first column), 3(second column), and 3.5 (third column) at critical moment.

case is attributed to the interaction of the horseshoe vortices from both piles in the region of the contracted flow. As stated before, horseshoe vortices are the result of the combination and interaction of the vortices from front face of the piles with the mean flow. The velocity and the strength of the mean flow are not constant, owing to shedding on the downstream of piles. Shedding is the reason of momentum exchange in the planes perpendicular to the Y direction. As known, shedding is not symmetry at the downstream of the piles with G/D around 2 (Sumner 2010), and as it is illustrated in Figure 13, present results show asymmetric velocity distribution in the case with $G/D = 2.5$. Therefore, flow velocities around both piles are not at the maximum value simultaneously. Asymmetric velocity around both piles in this case results in the creation of the horseshoe vortices with different strengths. Then, the strength of the interacted vortices is approximately between the strength of both horseshoe vortices. As stated in Figure 13 and previous studies (Sumner 2010), the flow and shedding in the case with $G/D = 3$ are symmetric. It means that the maximum flow velocities from both piles and the horseshoe vortices with the maximum strength occur at the same time. The interactions of these strong horseshoe vortices will result in the creation of a strong net-horseshoe vortex. The stronger horseshoe vortex results in higher velocity gradient, and then, higher shear stress exertion. On the case with $G/D = 3.5$, because of the larger distance between the piles, the horseshoe vortices have less interaction with each other. The Strouhal number for different spacing ratios is approximately the same, and the results show an acceptable consistency with the results of Akilli *et al.* (2004).

Summary and conclusions

The numerical analyses of flow patterns around single and side-by-side piles and the exerted shear stress on the bed in a turbulent flow regime are studied. The results showed the approximate dimensionless vortex shedding frequency (Strouhal number) of 0.21 for different cases at the downstream of side-by-side piles for flow Reynolds number of 10^5. For side-by-side piles, the case with $G/D = 3.5$ has a patch of a high value of vorticity at a higher elevation from the bed with respect to the other cases. By increasing the G/D, the oscillations at the downstream of each pile become symmetrical, and their amplitude become smaller. On the case of $G/D = 3$, the oscillation of V is stronger with a larger amplitude compared to other cases. For side-by-side piles, the critical G/D that leads to the largest shear stress exertion on the bed is found to be $G/D = 3$. The maximum bed shear stress on the case with $G/D = 3$ is 1.4 times larger than that of the single pile and 1.24 and 1.21 times larger than that of the cases with $G/D = 2.5$ and 3.5, respectively. Larger bed shear stress on the case with $G/D = 3$ can be attributed to the larger downward flow, larger oscillations of the vortices, and higher interaction of eddies.

The results of this study have significant practical applications for prediction, control, and prevention of scour-hole development around piles in engineering and environmental problems. Further study on the more complex geometries is required to advance the intuition of the flow pattern and the turbulent regime impacts on the scour development around complex man-made or natural structures.

Notation

The following symbols are used in this paper:

A	a fractional area open to flow (m^2)
c_p	a constant
c_f	a constant
$C_{\in 1}$,$C_{\in 2}$	constants
C_μ	a constant equals to 0.09
d	distance from wall in logarithmic law of wall (m)
D	pile diameter (m)
d_{50}	median particle size of sediment bed (mm)
f	vortex shedding frequency (1/s)
$F(x, y, z, t)$	VOF function
f_x, f_y, f_z	viscous accelerations in (X, Y, Z) directions, respectively (m/s^2)
F_{SOR}	a mass source

Fr	Froude number
g	acceleration due to gravity (m/s^2)
G	center-to-center distance between piles (m)
G_x, G_y, G_z	body accelerations in (X, Y, Z) directions, respectively (m/s^2)
h	depth of approach flow (m)
K	turbulent kinetic energy (m^2/s^2)
k_s	roughness height (m)
K_h, K_d, K_s, K_α, and K_t	the factors for flow depth-pile size, flow intensity, sediment size, pile shape, pile alignment, and time
K_1, K_2, K_3	correction factors for pier nose shape, angle of attack of the flow, and bed condition;
Q	flow discharge (m^3/s)
R_{DIF}	a turbulent diffusion term
Re	Reynolds number
R_{SOR}	a mass source
S_t	dimensionless vortex shedding frequency (Strouhal number)
t	time (s)
U, V, W	velocity components in (X, Y, Z) coordinates, respectively (m/s)
u_i,u_j,u_k	mean velocity along X, Y, and Z directions, respectively (m/s)
u_0	parallel component of velocity adjacent to the wall (m/s)
U_0	mean velocity of the approach flow (m/s)
U_c	critical velocity for initiation of sediments (m/s)
u_*	local shear velocity (m/s)
V_f	fractional volume
X, Y,Z	streamwise, transverse, and vertical directions, respectively
x_i, x_j, x_k	length in X,Y, and Z directions, respectively (m)
y_s	the maximum scour depth (m)
ε	turbulent dissipation rate (m^2/s^3)
k	von Karman constant
μ	fluid viscosity (N s/m^2)
μ_t	eddy viscosity (N s/m^2)
ξ	a term for definition of coordinate system
ρ	fluid density (kg/m^3)
σ_K	a constant equal to 1
τ_{ij}	Reynolds-stress tensor (N/m^2)

Acknowledgements

We wish to thank Mr Aslani-Kordkandi for his great efforts on experimental investigations. The authors wish to thank the Editor Professor James Ball and also three anonymous reviewers for their constructive comments which helped to improve the final manuscript.

Disclosure statement

No potential conflict of interest was reported by the authors.

References

Ahmed, F. and Rajaratnam, N., 1998. Flow around bridge piers. *Journal of Hydraulic Engineering*, 124 (3), 288–300.

Akbari, M.H. and Price, S.J., 2005. Numerical investigation of flow patterns for staggered cylinder pairs in cross-flow. *Journal of Fluids and Structures*, 20, 533–554.

Akilli, H., Akar, A., and Karakus, C., 2004. Flow characteristics of circular cylinders arranged side-by-side in shallow water. *Flow Measurement and Instrumentation*, 15, 187–197.

Ali, K.H.M. and Karim, O., 2002. Simulation of flow around piers. *Journal of Hydraulic Research*, 40, 161–174.

Arneson, L.A., *et al*., 2012. *Evaluating scour at bridges*. 5th ed. Hydraulic Engineering Circular No. 18 (HEC-18). Washington, DC: Federal Highway Administration.

Ataie-Ashtiani, B. and Aslani-Kordkandi, A., 2012. Flow field around side-by-side piers with and without a scour hole. *European Journal of Mechanics – B/Fluids*, 36, 152–166.

Ataie-Ashtiani, B. and Aslani-Kordkandi, A., 2013. Flow Field Around Single and Tandem Piers. *Flow, Turbulence and Combustion*, 90 (3), 471–490.

Ataie-Ashtiani, B., Baratian-Ghorghi, Z., and Beheshti, A.A. 2010. Experimental investigation of clear-water local scour of compound piers. *Journal of Hydraulic Engineering*, 136 (6), 343–351.

Ataie-Ashtiani, B. and Beheshti, A.A., 2006. Experimental investigation of clear-water local Scour at Pile Groups. *Journal of Hydraulic Engineering*, 132 (10), 1100–1104.

Bao, Y., Wu, Q. and Zhou, D., 2012. Numerical investigation of flow around an inline square cylinder array with different spacing ratios. *Computers & Fluids*, 55, 118–131.

Bao, Y., Zhou, D. and Tu, J., 2013. Flow characteristics of two in-phase oscillating cylinders in side-by-side arrangement. *Computers & Fluids*, 71, 124–145.

Baranya, S., *et al*., 2012. Three-dimensional RANS modeling of flow around circular piers using nested grids. *Engineering Application of Computational Fluid Mechanics*, 6, 648–662.

Bauer, W.J., 1954. Turbulent boundary layer on steep slopes. *Transactions of ASCE*, 119, 1212–1242.

Baykal, C., *et al*., 2015. Numerical investigation of flow and scour around a vertical circular cylinder. *Philosophical Transactions of the Royal Society A: Mathematical, Physical and Engineering Sciences*, 373, 20140104.

Beheshti, A.A. and Ataie-Ashtiani, B., 2010. Experimental Study of Three Dimensional Flow Field around a Complex Bridge Pier. *Journal of Engineering Mechanics*, 136 (2), 143–154.

Beheshti, A. A. and Ataie-Ashtiani, B., 2016a. Discussion of "Neuro-fuzzy GMDH systems based evolutionary algorithms to predict scour pile groups in clear water conditions" by M. Najafzadeh. *Ocean Engineering*, 123, 249–252.

Beheshti, A. A. and Ataie-Ashtiani, B., 2016b. Scour hole influence on turbulent flow field around complex bridge piers. *Flow, Turbulence and Combustion*, 97 (2), 451–474.

Beheshti, A.A., Ataie-Ashtiani, B., and Khanjani, M., 2013. Discussion of clear-water local scour around pile groups in shallow-water flow by Ata Amini, Bruce W. Melville, Thamer M. Ali, and Abdul H. Ghazali. *Journal of Hydraulic Engineering*, 139 (6), 679–680.

Bennett, J.P., 1995. Algorithm for resistance to flow and transport in sand-bed channels. *Journal of Hydraulic Engineering*, 121 (8), 578–590.

Bosch, G. and Rodi, W., 1998. Simulation of vortex shedding past a square cylinder with different turbulence models. *International Journal for Numerical Methods in Fluids*, 28 (4), 601–616.

Bouma, T.J., *et al*., 2013. Organism traits determine the strength of scale-dependent bio-geomorphic feedbacks: a flume study on three intertidal plant species. *Geomorphology*, 180–181, 57–65.

Carmo, B.S. and Meneghini, J.R., 2006. Numerical investigation of the flow around two circular cylinders in tandem. *Journal of Fluids and Structures*, 22, 979–988.

Coleman, S.E., 2005. Clearwater local scour at complex piers. *Journal of Hydraulic Engineering*, 131 (4), 330–334.

Dargahi, B., 1989. The turbulent flow field around a circular cylinder. *Experiments in Fluids*, 8, 1–12.

Dargahi, B., 1990. Controlling mechanism of local scouring. *Journal of Hydraulic Engineering*, 116 (10), 1197–1214.

Dey, S. and Raikar, R.V., 2007. Characteristics of Horseshoe Vortex in Developing Scour Holes at Piers. *Journal of Hydraulic Engineering*, 133 (4), 399–413.

Dubief, Y. and DeIcayre, F., 2000. On coherent-vortex identification inturbulence. *Journal of Turbulence*, I, 1–11.

Flow Science Inc. 2012. FLOW-3D, v10.0, User Manual, Santa Fe, USA.

Ge, L., Lee, S.O., Sotiropoulos, F., and Sturm, T., 2005. 3D unsteady RANS modeling of complex hydraulic engineering flows, II: model validation and flow physics. *Journal of Hydraulic Engineering*, 131 (9), 809–820.

Ge, L. and Sotiropoulos, F., 2005. 3D unsteady RANS modeling of complex hydraulic engineering flows. *Journal of Hydraulic Engineering*, 131 (9), 800–809.

Gopalan, H. and Jaiman, R., 2015. Numerical study of the flow interference between tandem cylinders employing non-linear hybrid URANS–LES methods. *Journal of Wind Engineering and Industrial Aerodynamics*, 142, 111–129.

Hannah, C.R., 1978. Scour at pile groups, Research Rep. No. 28-3. Civil Eng. Dept., University of Canterbury, New Zealand.

Hirt, C.W. and Nicholas, B.D., 1981. Volume of Fluid (VOF) method for the dynamics of free boundaries. *Journal of Computational Physics*, 39, 201–205.

Huang, W., Yang, Q., and Xiao, H., 2009. CFD modeling of scale effects on turbulence flow and scour around bridge piers. *Computers & Fluids*, 38, 1050–1058.

Khosronejad, A., Kang, S., and Sotiropoulos, F., 2012. Experimental and computational investigation of local scour around bridge piers. *Advances in Water Resources*, 37, 73–85.

Kirkil, G., Constantinescu, S.G., and Ettema, R., 2008. Coherent Structures in the Flow Field around a Circular Cylinder with Scour Hole. *Journal of Hydraulic Engineering*, 134 (5), 572–587.

Lam, K., Gong, W.Q., and So, R.M.C., 2008. Numerical simulation of cross-flow around four cylinders in an in-line square configuration. *Journal of Fluids and Structures*, 24, 34–57.

Lança, R., *et al.*, 2013. Clear-water Scour at Pile groups. *Journal of Hydraulic Engineering*, 139 (10), 1089–1098.

Liu, Y., *et al.*, 2001. Numerical studies of two side-by-side elastic cylinders in a cross-flow. *Journal of Fluids and Structures*, 15, 1009–1030.

Melville, B.W., 1975. Local scour at bridge sites. Rep. No. 117, U. o. Auckland ed., Auckland, New Zealand.

Melville, B.W. and Coleman, S.E., 2000. Bridge Scour. W. R. p. LLC ed., Colorado, USA.

Nikora, V. and Goring, D., 2000. Flow turbulence over fixed and weakly mobile gravel beds. *Journal of Hydraulic Engineering*, 126 (9), 679–690.

Palau-Salvador, G., Stoesser, T., and Rodi, W., 2008. LES of the flow around two cylinders in tandem. *Journal of Fluids and Structures*, 24, 1304–1312.

Papaioannou, G.V., *et al.*, 2008. On the effect of spacing on the vortex-induced vibrations of two tandem cylinders. *Journal of Fluids and Structures*, 24, 833–854.

Richardson, J.E. and Panchang, V.G., 1998. Three-dimensional simulation of scour-inducing flow at bridge piers. *Journal of Hydraulic Engineering*, 124 (5), 530–540.

Roulund, A., *et al.*, 2005. Numerical and experimental investigation of flow and scour around a circular pile. *Journal of Fluid Mechanics*, 534, 351–401.

Salaheldin, T.M., Imran, J., and Chaudhry, M.H., 2004. Numerical Modeling of three-dimensional flow field around circular piers. *Journal of Hydraulic Engineering*, 130 (2), 91–100.

Salim, M. and Jones, J.S., 1998. Scour around exposed pile foundations. North American Water and Environment Congress. Proceedings of the ASCE, 1998, Anaheim, CA.

Sheppard, D.M., Odeh, M., and Glasser, T., 2004. Large scale clear-water local pier scour experiments. *Journal of Hydraulic Engineering*, 130 (10), 957–963.

Smith, H.D. and Foster, D.L., 2005. Modeling of flow around a cylinder over a scoured bed. *Journal of Waterway, Port, Coastal, and Ocean Engineering*, 131 (1), 14–24.

Snyder, W.H. and Castro, I.P., 1999. Acoustic Doppler velocimeter evaluation in stratified towing tank. *Journal of Hydraulic Engineering*, 125 (6), 595–603.

Song, T. and Chiew, Y.M., 2001. Turbulence measurement in nonuniform open channel flow using Acoustic Doppler Velocimeter (ADV). *Journal of Engineering Mechanics*, 127 (3), 219–232.

Sumner, D., 2010. Two circular cylinders in cross-flow: a review. *Journal of Fluids and Structures*, 26, 849–899.

Sumner, D., *et al.*, 1999. Fluid Behavior of side-by-side circular cylinders in steady cross-flow. *Journal of Fluids and Structures*, 13, 309–338.

Vandenbruwaene, W., *et al.*, 2011. Flow interaction with dynamic vegetation patches: implications for biogeomorphic evolution of a tidal landscape. *Journal of Geophysical Research: Earth Surface*, 116, F01008.